In vitro and *in vivo* evaluation of an electrospun-aligned microfibrous implant for *Annulus fibrosus* repair

Maude Gluais[a,b], Johann Clouet[a,b,c,d], Marion Fusellier[a,e], Cyrille Decante[a,f],
Constantin Moraru[a,g], Maeva Dutilleul[a,b,h], Joëlle Veziers[a,b,h,i], Julie Lesoeur[a,b,h],
Dominique Dumas[j,k], Jérôme Abadie[l], Antoine Hamel[a,f], Eric Bord[a,g], Sing Yian Chew[m,n],
Jérôme Guicheux[a,b,i], Catherine Le Visage[a,b,*]

[a] *Inserm, UMR 1229, RMeS, Regenerative Medicine and Skeleton, Université de Nantes, ONIRIS, Nantes, F-44042, France*
[b] *Université de Nantes, UFR Odontologie, Nantes, F-44042, France*
[c] *CHU Nantes, Pharmacie Centrale, PHU 11, Nantes, F-44093, France*
[d] *Université de Nantes, UFR Sciences Biologiques et Pharmaceutiques, Nantes, F-44035, France*
[e] *Department of Diagnostic Imaging, CRIP, ONIRIS, College of Veterinary Medicine, Food Science and Engineering, Nantes, F-44307, France*
[f] *CHU Nantes, Service de Chirurgie Infantile, PHU5, Nantes, F-44093, France*
[g] *CHU Nantes, Service de Neurotraumatologie, PHU4 OTONN, Nantes, F-44093, France*
[h] *INSERM, UMS 016, CNRS 3556, Structure Fédérative de Recherche François Bonamy, SC3M Facility, CHU Nantes, Université de Nantes, Nantes, F-44042, France*
[i] *CHU Nantes, PHU4 OTONN, Nantes, F-44093, France*
[j] *Ingénierie Moléculaire et Physiopathologie Articulaire (IMoPA), UMR 7365 CNRS - Université de Lorraine, Vandœuvre-lès-Nancy, F54505, France*
[k] *UMS2008 IBSLor - CNRS-UL-INSERM Plateforme d'Imagerie et de Biophysique Cellulaire PTIBC-IBISA, Vandœuvre-lès-Nancy, F54505, France*
[l] *Animal Cancers as Models for Research in Comparative Oncology (AMaROC), ONIRIS, College of Veterinary Medicine, Food Science and Engineering, Nantes, F-44307, France*
[m] *School of Chemical and Biomedical Engineering, Nanyang Technological University, 637459, Singapore*
[n] *Lee Kong Chian School of Medicine, Nanyang Technological University, 308232, Singapore*

ARTICLE INFO

ABSTRACT

Annulus fibrosus (AF) impairment is associated with reherniation, discogenic pain, and disc degeneration after surgical partial discectomy. Due to a limited intrinsic healing capacity, defects in the AF persist over time and it is hence necessary to adopt an appropriate strategy to close and repair the damaged AF. In this study, a cell-free biodegradable scaffold made of polycaprolactone (PCL), electrospun, aligned microfibers exhibited high levels of cell colonization, alignment, and AF-like extracellular matrix deposition when evaluated in an explant culture model. The biomimetic multilayer fibrous scaffold was then assessed in an ovine model of AF impairment. After 4 weeks, no dislocation of the implants was detected, and only one sample out of six showed a partial delamination. Histological and immunohistochemical analyses revealed integration of the implant with the surrounding tissue as well as homogeneously aligned collagen fiber organization within each lamella compared to the disorganized and scarcer fibrous tissue in a randomly organized control fibrous scaffold. In conclusion, this biomimetic electrospun implant exhibited promising properties in terms of AF defect closure, with AF-like neotissue formation that fully integrated with the surrounding ovine tissue.

1. Introduction

Low back pain (LBP) is a major health issue that causes disability as well as a very substantial socioeconomic burden (as much as $253 billion dollars annually in the United States alone) [1,2]. Impairment of the *Annulus fibrosus* (AF) structural integrity, arising either by biological remodeling or by repetitive/traumatic events, is believed to be one of the main causes of LBP [3–7]. Indeed, neovascularization and neoinnervation, infiltrating the intervertebral disc (IVD) through peripheral AF lesions, can give rise to discogenic pain [8,9], while extensive AF radial tears may lead to IVD herniation and subsequently radicular pain [10]. The most common surgical procedure to treat IVD herniation is called partial discectomy or herniectomy and it consists of removal of the herniated tissue to relieve radicular pain. However, despite

---

successful pain relief and improved function, 25% of patients experience long-term unsatisfactory outcomes [11,12]. Indeed, untreated defects in the AF have been shown to persist over time due to the limited intrinsic healing capacity of the AF. Such defects are associated with up to 20% of postoperative reherniations and they increase the prevalence of IVD degeneration by 20% compared to the general population [11–20].

A limited number of procedures have been used for AF closure, including suturing and gluing techniques, which are considered to be relatively straightforward methods. However, neither simple suturing [21] nor more complex suture systems, such as the Dines knot [22] or Modified purse-string sutures [23,24], significantly reduce the reherniation rate or the degenerative processes in *ex* and *in vivo* ovine and porcine models. In addition, a two-year follow-up multicenter randomized controlled clinical study (NCT00760799) investigating the effect of an FDA-approved commercial suture technique, the Xclose™ tissue repair system (Annulex Technologies, Minnetonka, Minnesota, USA), found that there was no statistical reduction of postoperative pain or the reherniation rate in the treated group [25]. It is also important to point out that suturing techniques exhibit a number of major limitations, such as the creation of puncture holes and permanent stretching of the AF margins, which could induce additional tears and accelerate the degeneration process [26,27]. Likewise, few studies have investigated gluing techniques using either genipin-crosslinked fibrin gels [28–30], riboflavin-crosslinked high-density collagen gels [31,32], or isocyanate-terminated polyethylene glycol-trimethylene carbonate (PEG-TMC) gels [33] in *ex vivo* and *in vivo* models. Although there was strong adhesion to the surrounding tissue, with possible prevention of *Nucleus pulposus* (NP) herniation, only partial biomechanical restoration was achieved, with a disorganized fibrous tissue repair and no prevention of IVD degeneration. A combination of suturing and gluing techniques improved closure efficiency in a calf *ex vivo* model compared to the use of adhesive or sutures alone. This combined fixation technique has been shown to fail, however, after 100,000 cycles of load, thereby demonstrating its unsuitability for long-term AF sealing [34].

In this context, the use of implant devices appears to be a promising alternative strategy since they can fill AF defects without damaging the surrounding tissue and they can induce tissue repair. The commercial implant Barricaid™ (Intrinsic Therapeutics, Woburn, Massachusetts, USA) has exhibited promising short-term outcomes (2 years) in clinical evaluations, with a reduction in leg and back pain, preserved disc height, and a reduced risk of symptomatic reherniation (NCT01283438) [35,36]. This device is currently undergoing evaluation in two post-market surveillance registries (NCT03366779 and NCT03180749). However, its invasive implantation method using anchorage to the adjacent vertebrae with a titanium insert is reason for concern due to possible endplate lesions [37] and osteophyte formation at the anchorage site, as has already been reported for other experimental vertebral-anchored annular devices [38]. To overcome the lack of clinically effective therapies, a large number of natural and/or synthetic implants for AF closure have been investigated *in vivo* such as a synthetic poly (lactic-co-glycolic acid) sponge [39], a small intestinal submucosa implant [38], and a textile polyglycolic acid/polyvinylidene fluoride implant [40]. Cell recruitment and collagen deposition have been shown to take place within these implants. In addition, numerous *in vitro* studies have highlighted that the scaffold topography guides the induction of hierarchical organization of bone marrow mesenchymal stem cells (BMSCs), AF cells, and extracellular matrix (ECM) deposition [41–43].

Taken together, these results highlight the need for implants that function as a 3D scaffold that can mimic the complex native AF structure and that can guide cell migration, proliferation, and production of an AF-like tissue that can in turn fully integrate with the surrounding tissue. However, due to the inherent complexity of the AF tissue, designing such an implant remains a challenge. Specifically, the AF is an anisotropic structure that is arranged in concentric lamellae, of 200–400 µm thickness in humans, and it is mainly composed of aligned and parallel collagen fibers and proteoglycans such as aggrecan. The collagen fibers are oriented obliquely at a precise angle of 60° to the vertical axis of the spine and this inclination alternates from left to right with each lamella. As a result, this confers a cross-ply structure that is essential for the biomechanical function of the AF [44,45]. Native AF cells are mostly elongated fibroblast-like cells that are aligned and parallel to each other and they produce mainly type I collagen [46,47]. Numerous *in vitro* studies, using a variety of scaffolds, have demonstrated that 3D printing and electrospinning technologies are particularly suitable for designing highly organized micro- or nano-fibrous AF implants [48–50]. Polycaprolactone (PCL) in particular, which is a biocompatible and slowly biodegradable material with high mechanical properties that has already been used in numerous tissue engineering strategies and clinical applications, has been widely recommended for AF repair [41,42,51–59]. To our knowledge, only two papers have described electrospun PCL implantation in a large animal model (pig lumbar IVD and goat cervical IVD). In a recent elegant paper, a complex multilayer PCL scaffold, obtained by a combination of electrospinning and 3D printing technologies and sutures, was used successfully to repair an AF defect in pigs [60]. In the second paper, agarose hydrogel for NP, electrospun PCL for AF and porous PCL for endplates were combined and implanted in a goat cervical model for up to 8 weeks. Although this full disc replacement strategy aimed at treating patients who undergo total discectomy, where both damaged NP and AF are surgically removed, it confirmed the relevance of electrospun PCL for AF repair [61]. In this scarce literature context, the present study aimed to develop an electrospinning technology to design an aligned electrospun PCL scaffold that mimics the singular structure of native AF tissue. The objective of this study was to determine whether this cell-free, aligned, electrospun PCL scaffold could induce spontaneous organized fibrous tissue formation *in vitro*, in an original *ex vivo* model and in a sheep lumbar model. The aligned scaffold was compared to a randomly organized electrospun scaffold as a control for AF-like tissue formation.

2. Materials and methods

2.1. Fibrous scaffold fabrication

Random and aligned non-woven fibrous scaffolds of poly(ε-caprolactone) (PCL, Mn 80,000, Sigma-Aldrich, St. Quentin Fallavier, France) were produced by electrospinning. PCL was dissolved in 2,2,2-Trifluoroethanol (TFE, Sigma-Aldrich) at concentrations of 14 and 18 wt% for random and aligned scaffolds, respectively. One mL of PCL solution was loaded into a syringe that was attached to a 22-gauge blunt-end stainless steel needle and dispensed at a flow rate of 1 mL/h using a syringe pump (BSP-99 M, Linari Engineering, Pisa, Italy). To collect the PCL fibers, a 13-cm diameter rotating wheel (kindly provided by Prof. SY Chew, Nanyang Technological University, Singapore) attached to a DC motor (07SP-9032, Xajong Co., Ltd., Taichung, Taiwan) and regulated by a speed controller (XJC220-90C-B, Xajong Co.) was covered with aluminum foil and placed 10 cm from the tip of the needle. To obtain random fibers, which served as controls in this study, the needle was charged to +4.5 kV using a high-voltage positive generator (HVG-P60-WEB, Linari Engineering, Pisa, Italy), while the wheel, rotating at ~320 rpm, was charged to −4 kV using a high-voltage negative generator (ES30N-10 W, Gamma High Voltage Research Inc., Ormond Beach, Florida, USA). To obtain aligned oriented fibers, the needle was charged to +5 kV, while the wheel, rotating at ~2400 rpm, was charged to −4 kV. Electrospun materials were obtained in conditions with temperature ranging from 20.8 °C to 25.0° and humidity ranging from 31% to 55%.

2.2. Fibrous scaffold characterization

2.2.1. Structural evaluation

Random and aligned scaffolds were coated with gold-palladium using a Desk III Sputter Coater (Denton Vacuum, Moorestown, New Jersey, USA) and the surface morphology was examined by back-scattering of electrons using a Scanning Electron Microscope (SEM, LEO 1450VP®, Carl Zeiss, Marly Le Roi, France) at an acceleration voltage of 5 kV and 25 mA. The directionality (relative to the main axis) and the average diameters of random and aligned electrospun fibers (n = 3) were determined using ImageJ® (1.51s, National Institutes of Health, Bethesda, Maryland, USA).

To evaluate their thickness with ImageJ®, PCL scaffolds (n = 3) were snap frozen in liquid nitrogen and cryosectioned perpendicular to the direction of the collective wheel rotation with a scalpel. The samples were prepared for SEM as described above.

The pore size distribution and the porosity of the scaffolds were measured by mercury porosimetry (Autopore IV 9500®, Micromeritics Instrument Corp., Norcross, Georgia, USA). Dry scaffolds (40–70 mg) were placed in the chamber and air was removed from the pores. The samples (n = 3) were filled with mercury under reduced pressure (2 kPa), after which the pressure was incrementally increased to a maximum pressure of 30 kPa. The mercury intrusion volume was measured as the pressure increased, which allowed calculation of the pore size distribution within the samples and their overall porosity.

2.2.2. Mechanical testing

Uniaxial tensile testing was performed along the main fiber axis (the direction of the rotation during the electrospinning) using a texture analyzer (TA.HD*plus*, Stable Micro Systems®, Godalming, United Kingdom). The scaffold samples (n = 3) were cut into 90 × 11 mm rectangles, which were clamped with serrated grips and subjected to the following testing protocol: (1) preload to 0.1 N for 5 min; (2) 10 preconditioning cycles to 0.1% strain applied at a rate of 2 mm/s; and (3) elongation at a rate of 1 mm/s until failure. The strain was computed as the displacement normalized to the initial gauge length and the stress was calculated as the load normalized to the cross-sectional area. Young's Modulus was calculated as the slope of the linear portion of the stress-strain plot. The final tensile strength and maximum elongation were determined from the stress and the strain, respectively, before sample failure.

2.3. In vitro analysis

2.3.1. Sheep AF explant culture

In order to evaluate the spontaneous colonization of the implants when in contact with AF tissue after implantation, an *ex vivo* model was set-up. The PCL scaffolds were first cut into circular samples (1.5 cm in diameter) and decontaminated in 70% ethanol for 30 min, after which both sides of the scaffolds were exposed to UV radiation for 30 min. Prior to culture, the samples were coated with fetal bovine serum (FBS; Dominique Dutscher, Brumath, France) overnight in a humidified incubator at 37 °C and 5% CO_2.

Six female sheep (1-year-old) with an average body weight of 35 kg were used for the *in vitro* studies. The sheep were euthanized using an overdose of 140 mg/kg of pentobarbital (Dolethal®, Vetoquinol, France) and the IVDs were surgically isolated. AF tissues were carefully separated from NP tissues using a blade, diced into pieces (~0.5 × 1 cm), and rinsed in three consecutive baths of phosphate-buffered saline (PBS, Thermo Fisher Scientific, Illkirch, France) containing 2% penicillin-streptomycin solution (P/S, Invitrogen, Paisley, UK). The AF explants were subsequently placed on the FBS-coated PCL scaffolds and cultured in 24-well ultra-low attachment plates in Dulbecco's Modified Eagle Medium (Invitrogen DMEM containing high glucose, GlutaMAX™, and pyruvate) supplemented with 10% FBS, 1% P/S, and 0.17 mM of ascorbic acid (2-phospho-L-ascorbic acid trisodium salt, Sigma-Aldrich).

The medium was refreshed twice per week and the explants were cultured for 14 or 28 days.

2.3.2. Scaffold surface colonization

On day 14 and day 28, the AF explants were removed from the culture plates and the remaining scaffolds were fixed with 4% paraformaldehyde for 15 min at room temperature. The cells were permeabilized with 0.5% Triton X-100 in PBS, for 10 min at room temperature and then stained with phalloidin-Alexa Fluor® 568 (1:200 in PBS, Thermo Fisher Scientific) for 1 h at room temperature to visualize the cytoskeletal F-actin using a fluorescence microscope (Axio Zoom.V16, Carl Zeiss). The cytoskeletal staining was used to approximate the cell area and to determine the surface area of the scaffolds covered by the cells after 14 and 28 days of culture. The quantitative analyses were performed using ImageJ® software (N = 6, n = 3).

2.3.3. Cell proliferation

On day 14 and day 28, the AF explants were removed from the culture plates and the remaining scaffolds were incubated with 10 μM 5-ethynyl-2′-deoxyuridine (EdU) solution for 24 h and then fixed with 4% paraformaldehyde for 15 min at room temperature. EdU labeling and Hoechst staining were performed according to the manufacturer's specifications (ClickIT EdU®, Thermo Fisher Scientific). Visualization of the cell nuclei and cells displaying DNA-incorporated EdU was performed using a fluorescence microscope (Axio Zoom.V16). The quantitative analyses were performed using custom image-analysis software (N = 6, n = 3).

2.3.4. Cell morphology and phenotype

On day 14 and day 28, the AF explants were removed from the culture plates and the remaining scaffolds were processed for SEM microscopy. The scaffolds were fixed with 4% paraformaldehyde for 15 min at room temperature and then dehydrated with an ethanol gradient followed by two successive incubations in hexamethyldisilazane for 15 min (HMDS, Sigma-Aldrich). The dried scaffolds were coated with gold-palladium and observed using a SEM as previously described (N = 3, n = 1).

In a separate experiment, the scaffolds were fixed with 4% paraformaldehyde on day 14 and day 28. The cells were permeabilized with 0.5% Triton X-100® and non-specific sites blocked with 3% bovine serum albumin (BSA, Sigma-Aldrich) for 30 min. The cells were then stained with phalloidin-Alexa Fluor® 568 as previously described and then incubated overnight at 4 °C with anti-collagen type I primary antibody (1:250 in 1% BSA solution, Ab138492, rabbit monoclonal, Abcam, Cambridge, UK), or anti-aggrecan antibody (1:100 in 1% BSA, Ab1031, rabbit polyclonal, Merck Millipore, St. Quentin en Yvelines, France) and then with Alexa Fluor 488 secondary antibody (goat anti-rabbit IgG (H + L), 1:1000 in 1% BSA solution, Thermo Fisher Scientific) for 1 h at room temperature. The cell nuclei were stained with Hoechst and all of the samples were imaged using a confocal microscope (A1RS, Nikon, Champigny sur Marne, France). In addition, the reflection mode of the confocal microscope allowed visualization of the non-labeled underlying PCL scaffold. Quantitative analyses of the PCL fiber, F-actin, and collagen type I fiber directionalities were performed using ImageJ® software (N = 3, n = 1).

2.4. In vivo analysis

2.4.1. Ethical aspects and animals

Two female sheep (1-year-old; 29 and 36 kg, respectively, Vendée breed, GAEC HEAS farm, Ligné F-44850, France) were operated on in the accredited Centre of Research and Pre-clinical Investigations at the ONIRIS - National Veterinary School of Nantes with approval from the French Ministry of Agriculture and the ethics committee of the Région Pays de La Loire (Ethical number APAFIS 10,248). All animal experiments were carried out in accordance with the EU Directive 2010/63/

EU. Five lumbar IVDs (L1 - L2 to L5 - L6) per sheep were used for the experiments and the conditions were as follows: healthy group (2 IVD), unrepaired group (2 IVD), repaired group including randomly organized scaffold (3 IVD), and aligned scaffold (3 IVD).

2.4.2. Multilayer implant preparation

The PCL scaffolds were first cut into rectangular samples (2 × 5 mm), with the aligned scaffolds sectioned in order to have the prevailing fiber direction oriented at 30° to the long axis of the rectangle. The samples were first incubated in 70% ethanol for 30 min and then both sides were decontaminated by exposure to UV light for 30 min.

The day before the implantation, 50 mL of blood was drawn from the jugular vein, transferred into a sterile 50 mL polypropylene centrifuge tube and allowed to coagulate for 30 min at room temperature. The tubes were then centrifuged at 10,000 x g for 15 min and the serum was recovered. The PCL scaffolds were immediately incubated overnight in the serum solution in an incubator at 37 °C and 5% CO_2.

The serum-coated PCL samples were then stacked into multilayer constructs (2 mm height, ~8 to 10 layers) to mimic the multilamellar organization of native AF tissue. For aligned fibers, successive layers were assembled running in alternate directions, mimicking the angle-ply structure of the AF.

2.4.3. Surgery and tissue harvesting

Sheep anesthesia was induced by intravenous injection of 2–5 mg/kg of ketamine (Imalgene 1000®, Merial, Lyon, France) and 0.2 mg/kg of diazepam (Valium®, Roche, Boulogne-Billancourt, France), and maintained by inhalation of 1–3% isoflurane (Vetflurane®, Virbac, Carros, France) and intravenous injection of 1–3 mg/kg of propofol (PropoVet®; Abbott Laboratories Ltd., Maidenhead, UK). Analgesia was obtained by intravenous injection of 5 μg/kg of fentanyl (Abbott Laboratories Ltd.) and then continuously perfused at a rate of 5–20 μg/kg/h of fentanyl and 5–20 μg/kg/h of ketamine. The sheep were carefully bedded on their right side and their lumbar discs were exposed using a left retroperitoneal, transpsoas approach. Once exposed, five lumbar IVDs were randomly assigned to one of the four conditions: either no defect induction (healthy control group), a box annulotomy without implant deposition (unrepaired control group), a box annulotomy with deposition of a random multilayer implant (random group), or a box annulotomy with deposition of an aligned multilayer implant (aligned group). For the annulotomy groups, a ventro-lateral scalpel-induced box defect (2 × 5 mm and 2 mm depth) was created in the outer AF. All of the groups received an external polytetrafluoroethylene (PTFE) patch (1 × 1.25 cm, PTFE felt pledgets, 007976, Bard, Covington, Georgia, USA) glued on with cyanoacrylate adhesive (Leukosan® adhesive, 72,541-01, BSN Medical, Le Mans, France) to the adjacent vertebral bodies. Both sheep received 7 mg/kg of amoxicillin and clavulanic acid during the surgery then 1.75 mg/kg/d for 5 days and 0.5 mg/kg/d of meloxicam during the first 3 days.

After 4 weeks, the sheep were sacrificed under general anesthesia by intravenous injection of 140 mg/kg of pentobarbital. Lumbar spines were harvested and immediately fixed with 4% paraformaldehyde for 3 days at room temperature.

2.4.4. X-ray imaging and MRI

Pre-, post-operative, as well as pre-euthanasia X-ray imaging, was performed, as previously described [62], using a radiography machine (Convix 80® generator and Universix 120 table) from Picker International (Uniontown, Ohio, USA). Coronal and sagittal plane radiographs of the sheep lumbar spines were taken with a collimator-to-film distance of 100 cm, exposure of 100 mAs, and penetration power of 48 kVp.

Pre-, post-operative, as well as pre-euthanasia MRI of the entire lumbar sheep spines, were also performed as previously described [63] using a 1.5 T MRI scanner (Magnetom Essenza®, Siemens Medical

Solutions, Erlangen, Germany) with a standard spine coil to obtain T2-weighted images (TE: 86 ms, TR: 3000 ms; slice thickness: 3 mm) and T1-weighted images (TE: 12 ms, TR 322 ms; slice thickness: 3 mm).

The images were analyzed using Osirix software® (3.9, Osirix Foundation, Geneva, Switzerland). NP hydration was assessed by dividing the NP T2 signal in the middle axial position of the IVD by the T2 signal of the adjacent spinal cord in the same MRI slice. The disc height index (DHI) was measured as DHI = disc height/adjacent vertebral height on both the X-rays and the MRI.

2.4.5. Histological and immunohistochemical staining

PFA-fixed lumbar discs were decalcified for 72 h in a decalcifier (Shandon TBD-2™ Decalcifier, 6,764,004, Thermo Fisher Scientific), frozen for 3 min in isopentane/dry ice and then embedded in Super Cryoembedding Medium (SCEM) (Section Lab, Hiroshima, Japan) and frozen again in isopentane/dry ice until the SCEM set. The frozen samples were sectioned at −30 °C in the axial orientation into 7 μm sections using a cryostat (CryoStar NX70®, Thermo Fisher Scientific, Waltham, Massachusetts, USA). Following standard protocols, the sections were stained with Hematoxylin Eosin Safran (HES), Masson's trichrome (MT), and Picrosirius red (PR).

Immunostaining for type I collagen was performed using anti-collagen type I primary antibody (1:250 in 0.1% Triton and 4% BSA, Ab138492, rabbit monoclonal, Abcam, Cambridge, UK) and biotinylated goat anti-rabbit secondary antibodies (1:300 dilution, E0432, Dako, Agilent Technologies, Les Ulis, France). Briefly, sections were incubated with 0.1% trypsin (T9935, Sigma-Aldrich) solution for 30 min at 37 °C and then in freshly prepared 3% H_2O_2 solution to inactivate internal peroxidases. The sections were then blocked with 10% goat serum in 4% BSA for 30 min and incubated with the primary antibody overnight at 4 °C. Incubation with the corresponding biotin-labeled secondary antibody for 1 h was followed by 45 min of incubation with horseradish peroxide-conjugated streptavidin (1:400, P0397, Agilent Technologies). Antibody binding was visualized with diaminobenzidine (DAB, K3468, Agilent Technologies) as the HRP substrate, and the sections were counterstained for 30 s in hematoxylin. As a negative control, sections were processed using identical protocols but with omission of each primary antibody. All of the stained sections were observed using a slide scanner (Nanozoomer®, Hamamatsu Photonics, Hamamatsu, Japan) and all of the images were analyzed with NDP view2 software® (Hamamatsu Photonics).

2.4.6. Second harmonic generation

The second harmonic generation signal measurements were performed using an APE picoEmerald laser that delivered synchronized 7 ps pulses at λ = 800 nm to a scanning microscope (SP8-CARS, Leica Microsystems, Mannheim, Germany). In the SHG operation mode, the signal was filtered to detect collagen at 400 nm in the backward direction with a hybrid detector using a large dynamic range combined with low dark noise. The quantitative analyses of collagen fiber directionality were performed using ImageJ® software (n = 3).

2.5. Statistical analysis

All of the data are presented as means ± SEM. The statistical analyses were performed using Graph Pad Prism 5.0® software (GraphPad, San Diego, California, USA). Statistical significance was determined using two-way ANOVA followed by Bonferroni's post-test for multiple group comparisons with different variables (directionality), or a *t*-test for two-group comparisons (i.e., porosity, mechanical analysis, colonization, and proliferation). Statistical significance was set at $p < 0.05$. Unless otherwise stated, the experiments were repeated at least three times.
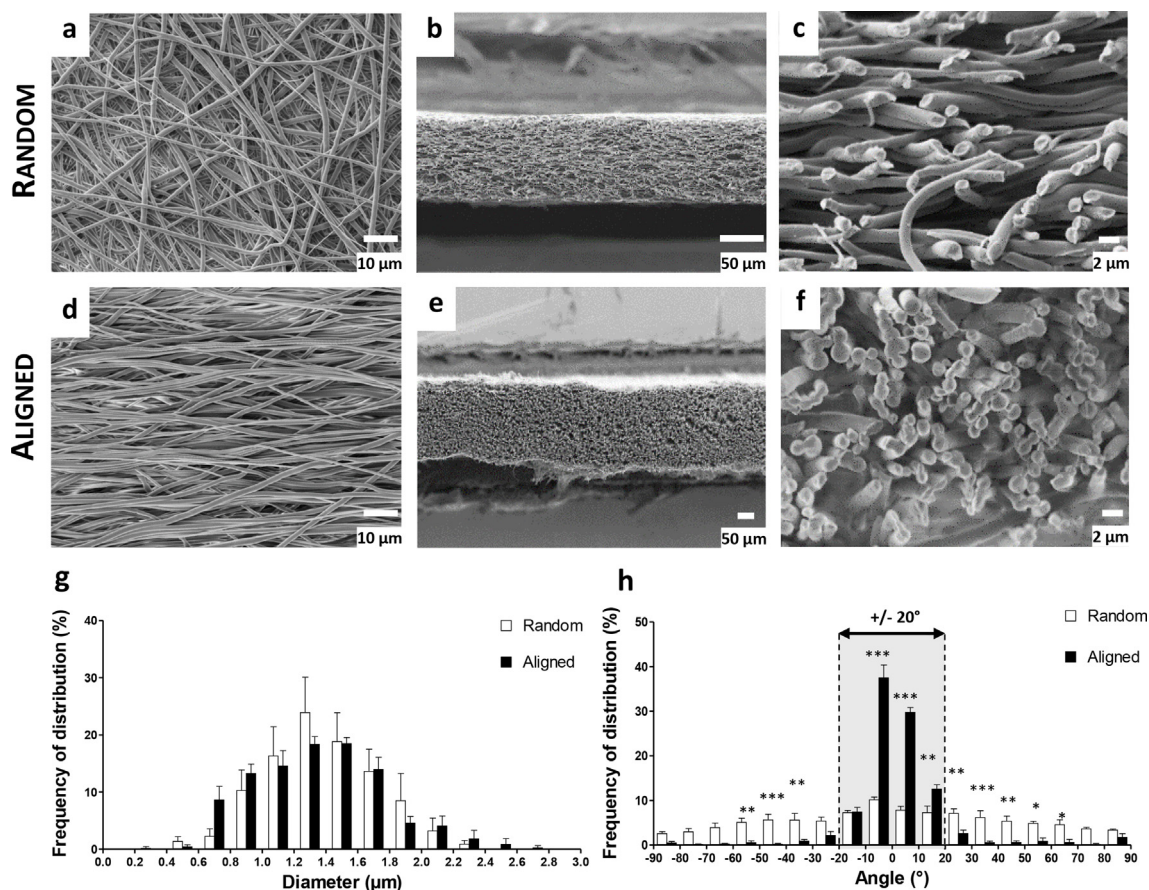
Fig. 1. Characterization of electrospun polycaprolactone (PCL) scaffolds. (a–f) Scanning electron microscopy (SEM) images of random and aligned scaffolds. Surfaces: (a, d) scale bar 10 μm. Cross-sections: (b, e) scale bar 50 μm, (c, f) scale bar 2 μm. (g) Diameter distribution and (h) angular distribution of the fibers in both of the scaffolds. The results are expressed as means ± SEM (n = 3) (***p < 0.001, **p < 0.01, statistical difference between random and aligned scaffolds).

3. Results

3.1. Fibrous scaffold characterization

Aligned and randomly organized fibrous scaffolds were successfully obtained by collecting electrospun fibers on a wheel rotating at high and low speed, respectively. SEM allowed visualization of both the surface and a cross-section of the scaffolds (Fig. 1). The cross-sectional images of the fibrous scaffolds revealed a homogeneous distribution of non-hollow, random, and aligned fibers throughout each scaffold (Fig. 1 b-c, e-f), with an average thickness of 81 ± 7 μm and 127 ± 8 μm, respectively. The SEM images allowed evaluation of both the diameter and the orientation of the constitutive PCL fibers in both of the scaffolds. The random and the aligned scaffolds displayed similar distributions of the fiber diameters (Fig. 1g), with average fiber diameters of 1.41 ± 0.36 μm and 1.33 ± 0.40 μm, respectively. In the aligned scaffolds, 88 ± 3% of the fibers (sum of the black boxes) were oriented at the same angle ± 20°, while most of the fibers in the random scaffolds did not appear to have a preferential orientation (only 33 ± 2%, sum of the white boxes) (Fig. 1h). The random and the aligned scaffolds had similar porosities of 84 ± 3% and 81 ± 1%, respectively, as determined by mercury porosimetry (data not shown).

Using uniaxial tensile tests, typical stress-strain curves were obtained for the fibrous scaffolds (data not shown) and the calculated mechanical properties were significantly different. The Young's moduli of the random and the aligned scaffold were calculated to be 16 ± 0.5 MPa *vs.* 55 ± 0.6 MPa (p < 0.0001), which corresponds to a significant 3.5-fold increase. The ultimate tensile strengths were 19 ± 2.9 MPa *vs.* 11 ± 0.6 MPa, respectively, (no significant

difference) and the failure strains were 545 ± 33% *vs.* 55 ± 6% (p < 0.0001), respectively.

3.2. In vitro analysis

3.2.1. Scaffold surface colonization and cell proliferation

Sheep AF tissue explants were deposited onto random and aligned scaffolds for 14 and 28 days (Fig. 2a) and cells colonizing the scaffold surfaces were identified by fluorescence microscopy imaging of the F-actin staining (Fig. 2b). Cell infiltration in the scaffolds was not evidenced. We then calculated the percentage of the scaffold surface covered by AF cells/cluster (Fig. 2c). On day 14, the AF cells covered 7.5 ± 1.1% and 8.2 ± 1.7% of the surface of random and aligned scaffolds, respectively (no statistical difference), while on day 28, there was an increase in the percentage of surface covered by cells on both types of surface, with no statistical difference between the two types of scaffold (50.0 ± 3.8% *vs.* 44.7 ± 3.2%, respectively).

The proliferation of AF cells on both types of scaffolds was investigated using a Click EdU assay, whereby incorporation of the modified thymidine analog EdU into newly synthesized DNA over a 24 h period was detected by fluorescence staining (Fig. 3). The percentage of cells with both Hoechst (nuclei) and EdU staining was found to be similar for the two types of scaffolds at both times (day 14: 56 ± 6% and 44 ± 8%, day 28: 31 ± 3% and 37 ± 4% for the aligned and the random scaffolds, respectively). Moreover, the total cell number on the scaffold surfaces was not statistically different for the random and the aligned scaffolds (data not shown), confirming the results obtained for the percentage of scaffold surface area covered by cells.
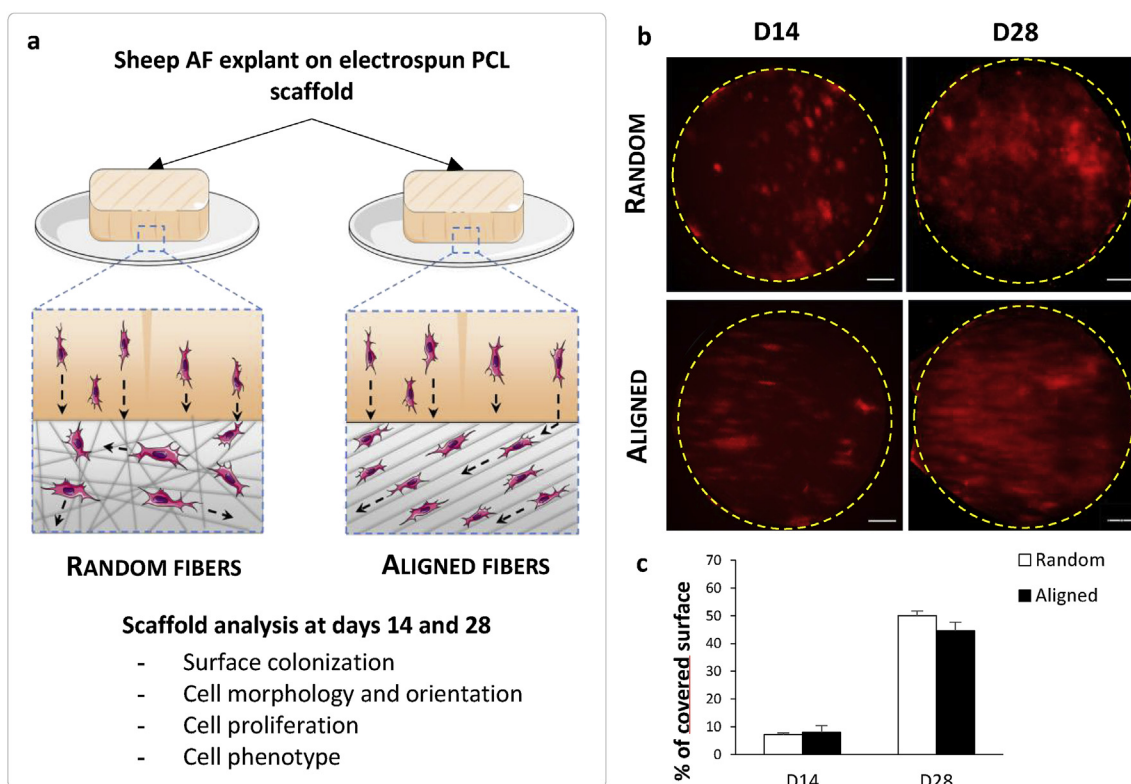
Fig. 2. In vitro culture on electrospun PCL scaffolds. (a) Schematic representation of the sheep Annulus fibrosus (AF) explant culture. Apposition of an AF tissue sample onto a random or an aligned scaffold. The cells could spontaneously colonize the PCL surface and orient themselves according to the underlying scaffold architecture. (b) On day 14 and day 28, the cells present on random and aligned surfaces (15 mm diameter, yellow dashed circles) were stained for F-actin (red) and imaged by fluorescence microscopy (scale bar 2 mm). (c) The percentage of PCL scaffold surface covered by the cells after 14 and 28 days of culture. The results are expressed as means ± SEM (N = 6, n = 3). (For interpretation of the references to colour in this figure legend, the reader is referred to the Web version of this article.)

3.2.2. Cell morphology, phenotype, and orientation

The cell morphology on the random and the aligned scaffolds was investigated by SEM and fluorescence microscopy to analyze the influence of scaffold architecture (Fig. 4a and b). The AF cells had an extensively spread morphology on both types of scaffold, with noticeable differences, however. On the random scaffolds, the cells were spread in all directions in an irregular manner, while on the aligned scaffolds, the cells were elongated with a spindle-shaped morphology typical of fibroblast-like cells and they were mostly oriented along the same direction of the underlying fibers. The orientation of the colonizing cells on both of the patterns was assessed by measurement of the direction of their actin filaments, while the reflection mode of the confocal microscope allowed visualization of the non-labeled PCL fibers. In the random group, similar to the underlying PCL fibers, the angular distribution of the F-actin exhibited no preferential fiber

orientation (Fig. 4c). In the aligned group, for convenience, the major axis of the PCL fibers was chosen as a reference and assigned a 0° angle. Similar to the angular distribution measured on the SEM images (Fig. 1g), the reflection mode showed that 87 ± 3% of the PCL fibers were oriented along the major axis ± 20°, while the phalloidin staining showed that 77 ± 2% of the F-actin was oriented in the same direction in the colonizing cells. This strongly suggests that there was a close correlation between the angular distribution of the actin filaments and that of the underlying PCL fibers.

Aggrecan and type I collagen, which are typically synthesized by AF cells, were investigated by immunostaining. On both types of scaffold, the cell cytoplasms were positively stained for aggrecan and type I collagen after 14 and 28 days of culture (data not shown). Moreover, fibrillar structures stained by anti-col I antibody were observed (Fig. 4a). Some stained fibers were found in areas devoid of F-actin,
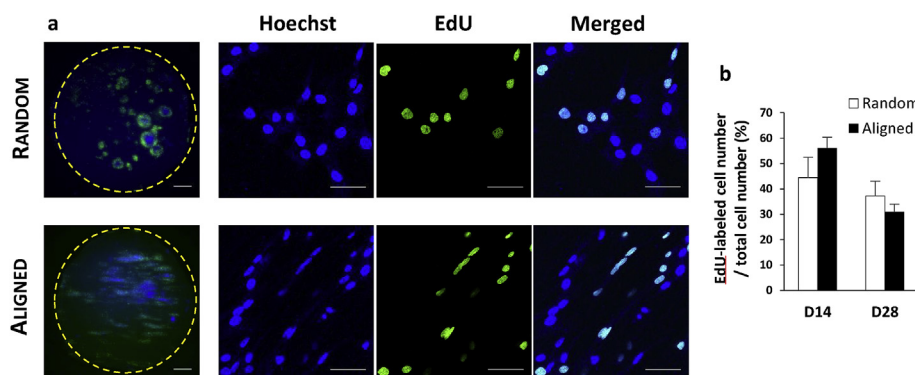

Fig. 3. AF cell proliferation on electrospun PCL scaffolds. (a) At days 14 and 28, AF cells were incubated 24 h with Click-iT® EdU solution. The cell nuclei were stained and random and aligned surfaces (15 mm diameter, yellow dashed circles) were imaged by fluorescence microscopy (scale bar 2 mm). Positive cells were identified by both Hoechst nuclear staining (blue) and fluorescent EdU (green) signal (scale bar 50 μm). (b) The percentage of positive EdU-labeled cells on both types of scaffolds on day 14 and day 28. The results are expressed as means ± SEM (N = 6, n = 3). (For interpretation of the references to colour in this figure legend, the reader is referred to the Web version of this article.)
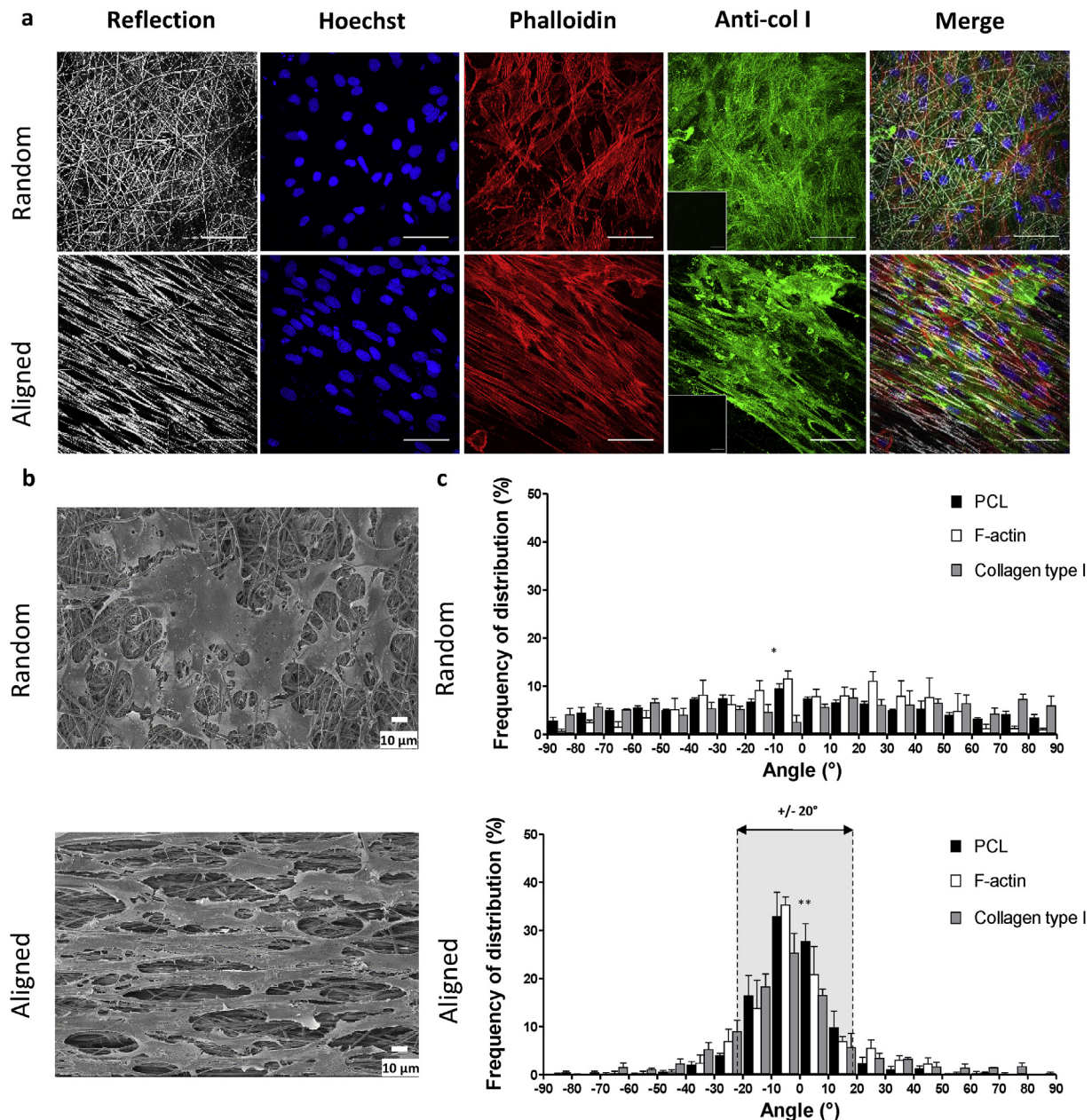
Fig. 4. Sheep AF cell morphology, phenotype, and orientation on electrospun PCL scaffolds. (a) Random and aligned scaffolds were processed and stained to visualize the PCL fibers (gray), nuclei (blue), F-actin (red), and type-I collagen (green) using confocal microscopy (day 28, scale bar 50 μm). Inserts are negative controls of collagen type I antibody (day 28, scale bar 50 μm). (b) Random and aligned scaffolds were processed and analyzed by SEM (scale bar 10 μm). (c) The angular distributions of the PCL fibers, F-actin, and type I collagen fibers at day 28 on random and aligned scaffolds. The results are expressed as means ± SEM (N = 3, n = 1) (**p < 0.01, *p < 0.05, statistical difference between PCL and collagen type I, no difference between PCL and F-actin). (For interpretation of the references to colour in this figure legend, the reader is referred to the Web version of this article.)

which strongly suggests that these fibers were extracellular (data not shown). While on random scaffolds, the angular distribution of these extracellular fibers revealed no preferential fiber orientation (Figs. 4c), 66 ± 5% of the positively stained extracellular fibers were oriented along the major axis of the underlying aligned scaffold ± 20°.

3.3. In vivo implantation

To assess the ability of our multilayer PCL scaffold to promote AF regeneration, an *in vivo* study was conducted in two sheep for 4 weeks. In lumbar discs, a defect was successfully created in the outer AF followed by implantation of random or aligned multilayer scaffolds with external PTFE patches to secure them (Fig. 5a).

3.3.1. X-ray imaging and MRI

There were no signs of surgery-related complications in the animals. X-rays and MRI taken preoperatively, postoperatively, and at one month were used to monitor lumbar disc heights and NP hydration. Quantitative analysis showed preservation of disc height at 4 weeks in both of the implanted groups as well as in the control groups (empty defect and uninjured disc) (data not shown). NP hydration was assessed using T2-weighted signal intensity measurements and there was no statistical difference between the various groups (data not shown). Moreover, 4 weeks after implantation, external PTFE patches were identified by MRI, which indicated that there had been no displacement compared to the postoperative images.
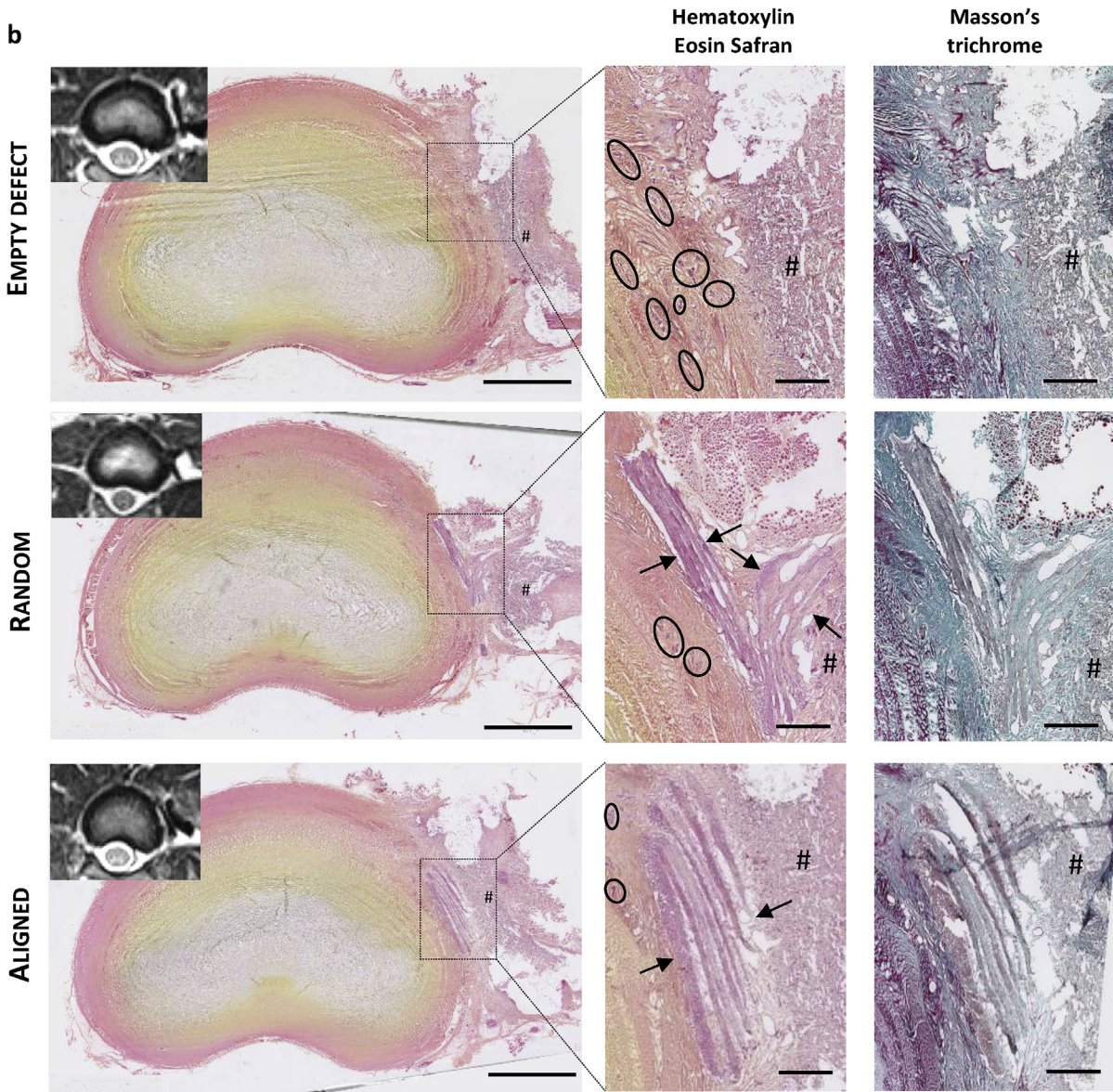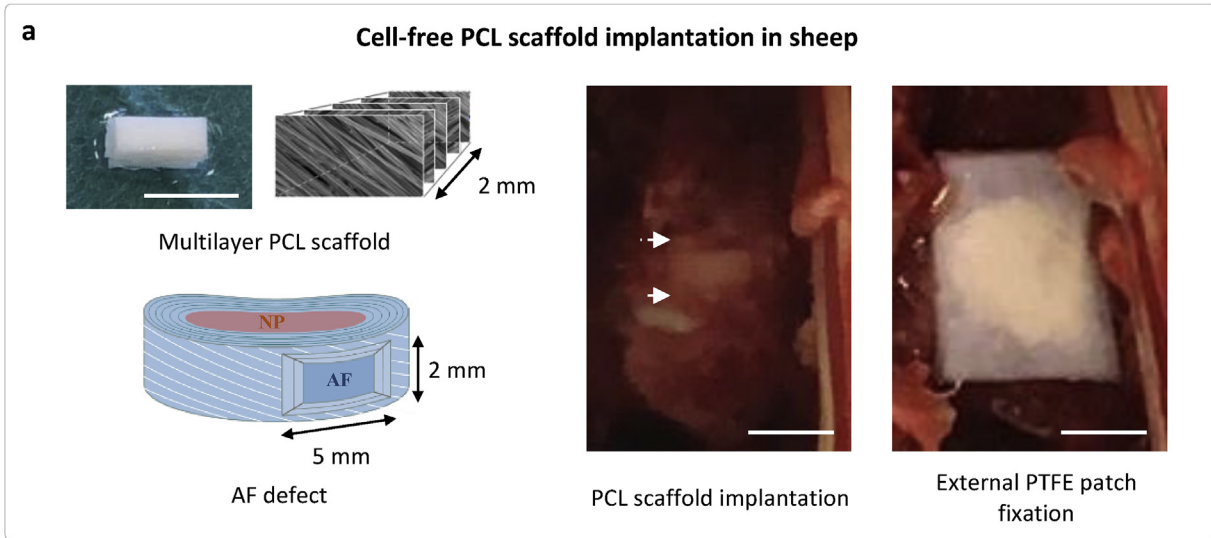
(caption on next page)

Fig. 5. In vivo study using an ovine model. (a) Experimental procedure. Using a left retroperitoneal approach, a scalpel-induced box defect (2 × 5 mm and 2 mm depth) was created in the outer annulus of lumbar discs (between the white arrows), and multilayer PCL implants (random or aligned) were implanted and secured in the defect by gluing an external polytetrafluoroethylene (PTFE) patch to the adjacent vertebral bodies (scale bar 5 mm). (b) MRI was performed 4 weeks after the surgery and intervertebral discs were explanted, cryo-sectioned, and histochemically stained with hematoxylin/eosin/safran (HES) and Masson's Trichrome (MT) (scale bar: 5 mm for full disc sections, 1 mm for high magnification sections; PTFE patch identified by #, vascular ingrowth identified in black circles).

3.3.2. Histological and immunohistochemical analyses

Histological staining of decalcified cryosectioned IVDs with HES and TM demonstrated retention of NP, with regular and intact inner AF lamellae (Fig. 5b). The location of the defect was confirmed to be in the outer AF. The empty defect exhibited irregular fibrous reparative tissue with numerous vascular ingrowths at 4 weeks. This tissue was highly cellularized with fibroblast-like cells displaying elongated nuclei. This collagen-rich tissue was disorganized with no preferential orientation of the neosynthesized collagen fibers. In both of the repaired groups (i.e., the random and the aligned group), the multilayer PCL scaffolds were well positioned within the outer AF defects without any sign of dislocation after 4 weeks of implantation. Only one randomly organized scaffold exhibited delamination of the superficial PCL layer. Both implants were well integrated into the surrounding AF, with continuous collagen fibers at the implant margins. There was no sign of pronounced foreign body reaction in the implant and in the region surrounding the implant. Homogeneous cell infiltration throughout the implants was observed and the cells had elongated nuclei, suggesting colonization by fibroblast-like cells. A regular fibrous tissue was observed inside the implants, between the PCL layers, and within each PCL layer, with very little vascular ingrowth.

Masson's trichrome and immunohistochemical staining of type I collagen revealed positively stained fibrous tissue in both the random and the aligned scaffolds, with noticeable differences between the two (Fig. 6a). The collagen fiber bundles in the aligned scaffolds appeared to be denser and more oriented compared to the ones in the random scaffolds. In addition, observation of picrosirius red staining under crossed polarizer revealed a strong birefringent intensity in the aligned scaffolds. The birefringence confirmed that the collagen fibers were aligned, which was not observed in the random scaffolds. Moreover, the collagen fibers within adjacent layers of the PCL were aligned along two opposing directions (Fig. 6a, white arrows), which closely replicates the cross-ply structure of native AF tissue. Consistent with the immunohistochemical staining, second harmonic generation microscopy revealed alignment of the collagen fibers within a single aligned PCL layer compared to a more disorganized and less dense collagen network in the random group. Quantitative analysis of the collagen orientation within a single PCL layer was performed on the SHG images of both scaffolds and was compared to that of native sheep AF tissue (Fig. 6b). For convenience, the major axis of the collagen fibers was systematically chosen as a reference and assigned a 90° angle. In native AF tissue, 92 ± 6% of the collagen fibers were oriented along the major axis ± 20°, while 87 ± 4% and only 50 ± 3% of the collagen fibers followed the same direction within a single layer of the aligned and the random scaffolds, respectively.

4. Discussion

The IVD has a pivotal role in spine kinematics. It provides stability during motion such as compression, distraction, sliding/twisting, and bending. IVD function results from the cooperative action of the NP and the AF to appropriately respond to a wide range of loads by contributing to the distribution and transmission of loads between the vertebral bodies. Any disruption in one of the IVD regions has a pronounced effect on the overall function of the IVD and hence on the stability of the spine.

AF damage is known to induce IVD degeneration and is one of the most extensively used methods for induction of IVD degeneration in animal models, including mice, rats, rabbits, dogs, pigs, and sheep [64].

These data showed that structural alteration of the AF is likely to induce leakage of the NP outside the IVD and to activate a cascade of cell-mediated responses, thereby leading to IVD degeneration [24,26,31,65–67]. AF lesions persist over time when left unrepaired and they may promote herniation of the NP tissue towards the spinal canal as well as a neural and vascular ingrowth within the defect [3–7,19].

Effective AF closure and repair would provide significant clinical benefits including the lessening of IVD degeneration, the prevention of IVD recurrent herniation associated with radicular pain, and prevention of neural and vascular ingrowth associated with discogenic pain. For these reasons, over the past decade, strategies for addressing IVD regeneration have increasingly focused on AF closure and repair. In this context, the objective of this study was to design an electrospun biomaterial that closely mimics the singular structure of native AF tissue and to assess its ability to appropriately repair AF defects in an ovine model. PCL is a biocompatible material with high mechanical properties that possess a very slow degradation rate (2–3 years depending on the starting molecular weight and form). The degradation of this semi-crystalline polyester has been reported in 2 steps, with first a hydrolytic cleavage of the ester bonds in the amorphous regions which releases a 6-hydroxycaproic acid that can be absorbed by the cells to be metabolized in the Krebs cycle and eliminated in the urine. The second stage, which is slower, concerns the intracellular degradation of crystalline domains by macrophages, giant cells and fibroblasts [51]. Therefore, PCL is particularly interesting for the preparation of implantable devices, where a low degradation rate is highly relevant for slow remodeling tissues such as AF.

The AF is arranged in concentric lamellae composed of aligned collagen fibers, which allow NP confinement by resisting tensile stretching [68]. We hypothesized that an effective AF repair material should approximate the ability of the native tissue to withstand the IVD mechanical environment and guide the neoformation of an AF-like tissue. The use of electrospinning technology in association with a collector wheel allowed production of aligned and randomly organized fibrous scaffolds with similar microsized PCL fibers and porosity. The random scaffold was chosen as a control group to monitor the *in vitro* and *in vivo* effect of micropattern orientation on AF cells. The aligned scaffold exhibited uniaxial tensile mechanical properties similar to those of a single AF lamella Young's Modulus (ranging from 31 to 65 MPa) [69]. To our knowledge, only two other studies to date have reported the development of materials with a similar tensile modulus, produced by electrospinning, alone or in association with 3D printing [42,70]. Thus, the use of electrospinning appears to be an appropriate strategy to design a scaffold with architectural and mechanical properties that match native AF tissue and that could sustain the complex IVD mechanical loads and provide stability at implantation.

In the current study, AF explant culture on electrospun scaffolds was used to assess the feasibility of developing an acellular electrospun scaffold for AF repair. To our knowledge, this is the first time that an explant culture model has been used to mimic the *in vitro* ability of AF cells present in the surrounding tissue to migrate, colonize, and proliferate on an implant. We demonstrated that the cells were able to colonize and proliferate on both types of scaffold surface, with increasing colonization of the surface area over time. No difference was seen between the random and the aligned scaffolds. This appears to indicate that once in contact with the PCL electrospun scaffold, the cells present in AF tissue can spontaneously populate and proliferate on the scaffold, irrespective of its architecture. The cell proliferation appeared
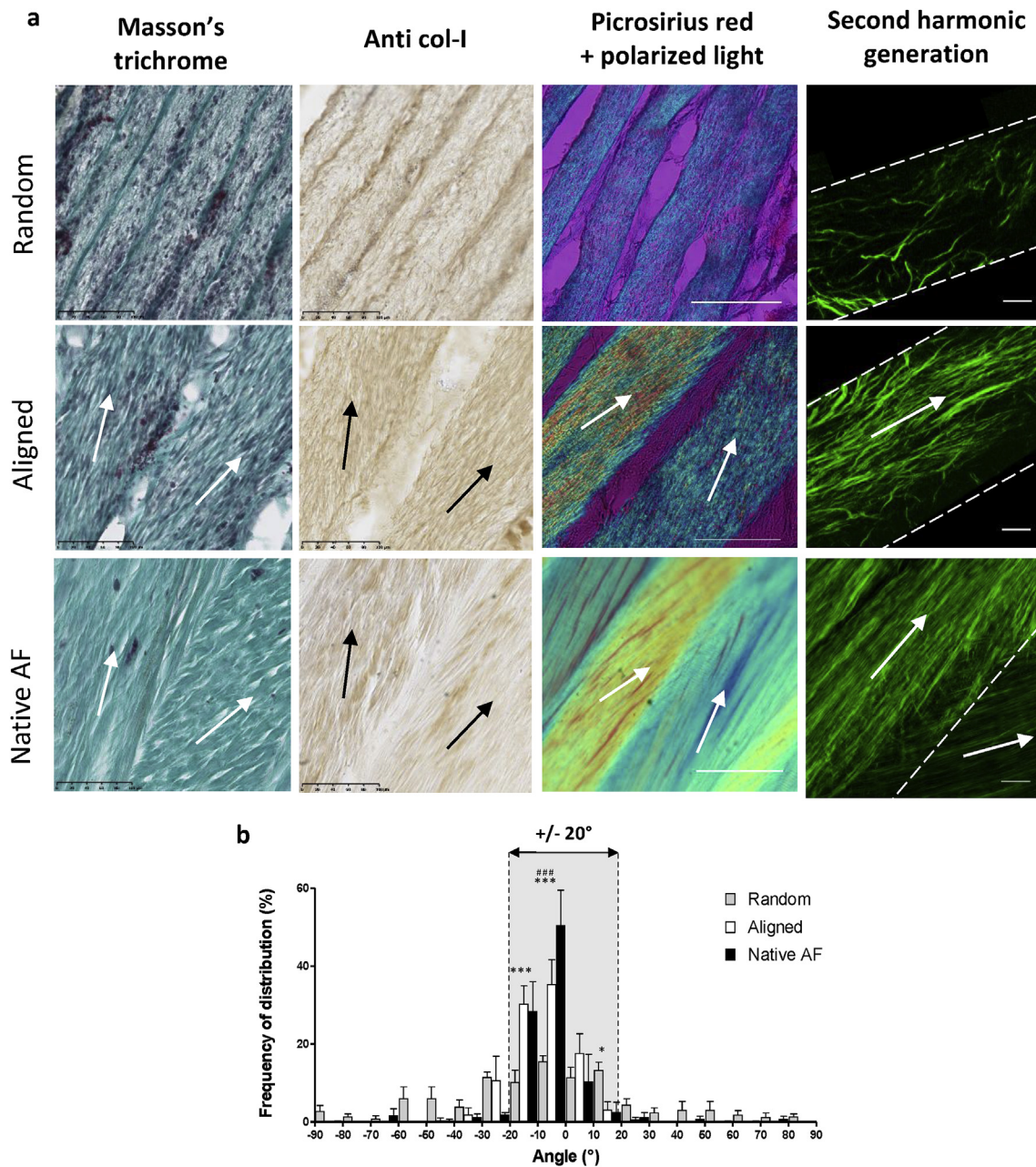
Fig. 6. Identification of neocollagen synthesis after 4 weeks of implantation. (a) Immunohistological staining with Masson's trichrome and anti-type I collagen of random and aligned implanted scaffolds (scale bar 100 μm). The picrosirius red staining in association with polarized microscopy allowed visualization of the collagen orientation (dashed arrow, scale bar 100 μm). The second harmonic generation microscopy allowed visualization of the collagen deposition within a single membrane (dashed line) (scale bar 20 μm). (b) The angular distributions of the collagen fibers within a single membrane of random and aligned scaffolds. The results are expressed as means ± SD (N = 1, n = 3) (###$p < 0.001$, statistical difference between native AF and aligned scaffold, ***$p < 0.001$, *$p < 0.05$ statistical difference between native AF and random scaffold). (For interpretation of the references to colour in this figure legend, the reader is referred to the Web version of this article.)

to have a tendency to decrease between day 14 and day 28, which could be explained by the increase in the covered scaffold surface. Observation of colonies on the surface of the scaffolds strongly suggests that, after an initial migration phase, cell proliferation could be a major factor for the increase of cell number and percentage of covered surface.

We next determined that the scaffold architecture strongly influenced the cell morphology and that it allowed maintenance of the cellular phenotype. As specific phenotypic markers of AF cells are still lacking, we analyzed the production of proteins such as type I collagen and aggrecan core protein. Both of these were synthesized by the cells on the random and the aligned scaffolds. The quantitative analysis

revealed a close match between the PCL fiber orientation and the cell cytoskeleton and subsequent extracellular type I collagen deposition. The cell morphology and the extracellular matrix (ECM) deposition pattern are in accordance with previous findings where micropatterned scaffolds were shown to exhibit contact guidance that induced cell and ECM alignment [19,56,71–77]. These results highlight the importance of mimicking the native AF architecture to first induce alignment of the cells and to then promote the deposition of an anisotropic ECM.

Random and aligned scaffolds were stacked into multilayer scaffolds to replicate the multilamellar structure of AF tissue. We then embarked on an ovine study to investigate whether the multilayer fibrous scaffolds could be tolerated by sheep and induce the formation of

anisotropic repair tissue without eliciting an inflammatory response. Sheep have been used extensively as an experimental model to investigate both IVD diseases and treatment strategies [32,38,40,64,78]. Indeed, sheep IVDs have numerous similarities with human IVDs including anatomy, size, cell population and, interestingly, biomechanical properties, which make this animal an ideal model to approximate the human IVD pathophysiology [79]. In our pilot study, a box-shaped defect was induced in the outer AF to allow the evaluation of our biomaterial in this specific region. Such a superficial defect was selected to avoid exposure to the NP pressure which often prevents maintenance of implants within the defect, thereby limiting the evaluation of the tissue repair within the implants [80,81]. After 4 weeks of implantation, all implant of the repaired groups (i.e., the random and the aligned groups) were successfully retained by use of external PTFE patches that were glued to the adjacent vertebrae, as indicated by the histological staining. However, it was noted that in one of the random groups, half of the PCL superficial layer appeared to have delaminated (Fig. 5b). MRI showed that the external patch was displaced in its ventral part. This was confirmed by histological staining, where muscle tissue was seen adjacent to the implant instead of the PTFE patch. It would appear that, upon implantation, the external patch was not properly fixed to the vertebral body, and its dislocation induced delamination of the multilayer scaffold underneath. This indicates the importance of a combined strategy to secure an AF repair implant within the defect. It is worth noting that although we aimed at replicating the AF cross-ply structure, PCL layers were stacked but not glued nor sutured to each other, thus facilitating the expected spontaneous cell infiltration. We also hypothesized that deposition of collagen fibers between the PCL layers might have induced the formation of a cohesive matrix that prevented a critical delamination of the layered implants. This anchoring strategy will need to be further evaluated in a full thickness defect, that corresponds to a herniated condition, where the implant will be exposed to the NP content.

To our knowledge, this *in vivo* study is the first to demonstrate, in a sheep lumbar model, a successful biological integration of electrospun PCL with the host's surrounding AF tissue, with no granuloma formation around the implants. Numerous cells were seen within each PCL layer of the random and the aligned scaffolds, suggesting that the implant porosities were sufficient to induce cell infiltration and tissue ingrowth throughout each layer. Newly formed collagen fibrous tissue was clearly observed within each implant, as evidenced by collagen type I staining. Observation by picrosirius red staining under polarized light and second harmonic generation allowed identification and quantification of the regular and the oriented collagen fibers within the aligned scaffold. Moreover, all of the histological analyses appear to show numerous and dense collagen fibers in the aligned scaffold, while fewer collagen fibers were deposited in the random scaffold *in vivo*. Dense fibrous repair tissue was also determined to be present in the empty group, indicating spontaneous healing of the superficial defect. However, histological observation revealed that the tissue was highly disorganized due to the absence of a guiding implant. This is in accordance with previous studies in sheep and rabbits reporting superficial healing of AF defects by deposition of a disorganized collagen tissue with mechanical properties that cannot withstand the physical loads that arise during the subject's lifetime [6,82–84]. The present *in vivo* study confirms the results obtained *in vitro* and it once again demonstrates the importance of contact guidance of the scaffold architecture for deposition of a highly organized repair tissue. Moreover, these results are in accordance with data recently reported in an *in vivo* porcine AF defect model using a PCL nano- and micro-sized multilayer fibrous scaffold. Similar to our study, this complex implant induced the deposition of aligned and well-integrated collagen fibers on the fibrous layers and a reduction of the degenerative process after 12 weeks of recovery [60]. Despite the use of different *in vivo* models, both studies demonstrated the potential of PCL-mimicking fibrous scaffolds for AF repair.

Further investigations should be undertaken to compare the mechanical properties of this newly formed fibrous tissue with native AF tissue and to evaluate its long-term efficiency in maintaining IVD structural and mechanical integrity. Finally, both the implant and the anchoring technique appear promising in this pilot study and could be translated into a herniated IVD model [40]. Indeed, implantation of a thicker multilayer aligned scaffold will be required to assess whether the scaffold can promote full-thickness AF repair, prevent NP herniation, and limit disc degeneration.

5. Conclusion

In this study, we successfully developed a cell-free PCL fibrous scaffold with morphological and mechanical properties that mimicked those of the native AF lamellae and that was able to promote spontaneous *in vitro* cell colonization, proliferation, and organization. Using an ovine model, we demonstrated that the aligned multilayer scaffold provided an essential inductive microenvironment for the production of collagen fibrous tissue that mimics the outer AF region. This implant could potentially act as a 3D scaffold that induces the production of AF-like tissue and that could prevent IVD recurrent herniation, as well as neural and vascular ingrowth, and that might also slow the IVD degeneration process.

Conflicts of interest

The authors declare no financial conflicts of interest.

Data availability

The raw/processed data required to reproduce these findings cannot be shared at this time due to technical limitations.

References

[1] D. Hoy, L. March, P. Brooks, F. Blyth, A. Woolf, C. Bain, G. Williams, E. Smith, T. Vos, J. Barendregt, C. Murray, R. Burstein, R. Buchbinder, The global burden of low back pain: estimates from the Global Burden of Disease 2010 study, Ann. Rheum. Dis. 73 (2014) 968–974.

[2] J. Dowdell, M. Erwin, T. Choma, A. Vaccaro, J. Iatridis, S.K. Cho, Intervertebral disk degeneration and repair, Neurosurgery 80 (2017) S46-S54.

[3] M. a Adams, W.C. Hutton, The mechanics of prolapsed intervertebral disc, Int. Orthop. 6 (1982) 249–253.

[4] M.A. Adams, B.J. Freeman, H.P. Morrison, I.W. Nelson, P. Dolan, Mechanical initiation of intervertebral disc degeneration, Spine (Phila. Pa. 1976) 25 (2000) 1625–1636.

[5] C.Y. Yu, K.H. Tsai, W.P. Hu, R.M. Lin, H.W. Song, G.L. Chang, Geometric and morphological changes of the intervertebral disc under fatigue testing, Clin. Biomech. 18 (2003) 3–9.

[6] J.C. Iatridis, J.J. MacLean, D.A. Ryan, Mechanical damage to the intervertebral disc annulus fibrosus subjected to tensile loading, J. Biomech. 38 (2005) 557–565.

[7] J.P. Callaghan, S.M. McGill, Intervertebral disc herniation: studies on a porcine model exposed to highly repetitive flexion/extension motion with compressive force, Clin. Biomech. 16 (2001) 28–37.

[8] Y.-S. Choi, Pathophysiology of degenerative disc disease, Asian Spine J 3 (2009)

39–44.

[9] P. Ramani, Section 2: basic knowledge in lumbar disc herniation, Textbook of Surgical Management of Lumbar Disc Herniation, JP Medical Ltd, 2013, pp. 11–50.

[10] C.-J. Chiang, C.-K. Cheng, J.-S. Sun, C.-J. Liao, Y.-H. Wang, Y.-H. Tsuang, The effect of a new anular repair after discectomy in intervertebral disc degeneration: an experimental study using a porcine spine model, Spine (Phila. Pa. 1976) 36 (2011) 761–769.

[11] M.J. McGirt, G.L. Garcés Ambrossi, G. Datoo, D.M. Sciubba, T.F. Witham, J.P. Wolinsky, Z.L. Gokaslan, A. Bydon, Recurrent disc herniation and long-term back pain after primary lumbar discectomy: review of outcomes reported for limited versus aggressive disc removal, Neurosurgery 64 (2009) 338–344.

[12] E.J. Carragee, A.O. Spinnickie, T.F. Alamin, S. Paragioudakis, A prospective controlled study of limited versus subtotal posterior discectomy: short-term outcomes in patients with herniated lumbar intervertebral discs and large posterior anular defect, Spine (Phila. Pa. 1976) 31 (2006) 653–657.

[13] M. Mariconda, O. Galasso, C. Milano, Frequency and clinical meaning of long-term degenerative changes after lumbar discectomy visualized on imaging tests, Eur. Spine J. 19 (2010) 136–143.

[14] J.E. Schroeder, J.R. Dettori, E.D. Brodt, L. Kaplan, Disc degeneration after disc herniation : are we accelerating the process ? Evid. Based Spine Care J. 3 (2012) 33–40.

[15] E.J. Carragee, A.S. Don, E.L. Hurwitz, J.M. Cuellar, J.A. Carrino, R. Herzog, ISSLS Prize Winner: Does discography cause accelerated progression of degeneration changes in the lumbar disc a ten-year matched cohort study, Spine (Phila. Pa. 1976) 34 (2009) 2338–2345.

[16] E. Yorimitsu, K. Chiba, Y. Toyama, K. Hirabayashi, Long-term outcomes of standard discectomy for lumbar disc herniation: a follow-up study of more than 10 years, Spine (Phila. Pa. 1976) 26 (2001) 652–657.

[17] R.L. Lebow, O. Adogwa, S.L. Parker, A. Sharma, J. Cheng, M.J. Mcgirt, Asymptomatic same-site recurrent disc herniation after lumbar discectomy results of a prospective longitudinal study with 2-year serial imaging, Spine (Phila. Pa. 1976) 3636 (2011) 2147–2151.

[18] J.A. Key, L.T. Ford, Experimental intervertebral-disc lesions, J. Bone Joint Surg. Am. 30A (1948) 621–630.

[19] C.C. Guterl, E.Y. See, S.B.G. Blanquer, A. Pandit, S.J. Ferguson, L.M. Benneker, D.W. Grijpma, D. Sakai, D. Eglin, M. Alini, J.C. Iatridis, S. Grad, Challenges and strategies in the repair of ruptured Annulus fibrosus, Eur. Cell. Mater. 25 (2013) 1–21.

[20] G. Vadalà, G. Sowa, M. Hubert, L.G. Gilbertson, V. Denaro, J.D. Kang, Mesenchymal stem cells injection in degenerated intervertebral disc: cell leakage may induce osteophyte formation, J. Tissue Eng. Regenerat. Med. 6 (2012) 348–355.

[21] B.D. Ahlgren, W. Lui, H.N. Herkowitz, M.M. Panjabi, J.P. Guiboux, Effect of anular repair on the healing strength of the intervertebral disc: a sheep model, Spine (Phila. Pa. 1976) 25 (2000) 2165–2170.

[22] A.H. Bateman, C. Balkovec, M.K. Akens, A.H.W. Chan, R.D. Harrison, W. Oakden, A.J.M. Yee, S.M. McGill, Closure of the Annulus fibrosus of the intervertebral disc using a novel suture application device – in vivo porcine and ex-vivo biomechanical evaluation, Spine J. 16 (2016) 889–895.

[23] Y.F. Chiang, C.J. Chiang, C.H. Yang, Z.C. Zhong, C.S. Chen, C.K. Cheng, Y.H. Tsuang, Retaining intradiscal pressure after annulotomy by different annular suture techniques, and their biomechanical evaluations, Clin. Biomech. 27 (2012) 241–248.

[24] C.H. Yang, Y.F. Chiang, C.H. Chen, L.C. Wu, C.J. Liao, C.J. Chiang, The effect of annular repair on the failure strength of the porcine lumbar disc after needle puncture and punch injury, Eur. Spine J. 25 (2016) 906–912.

[25] A. Bailey, A. Araghi, S. Blumenthal, G.V. Huffmon, Prospective, multicenter, randomized, controlled study of anular repair in lumbar discectomy: two-year follow-up, Spine (Phila. Pa. 1976) 38 (2013) 1161–1169.

[26] K. Masuda, Y. Aota, C. Muehleman, Y. Imai, M. Okuma, E.J. Thonar, G.B. Andersson, H.S. An, A novel rabbit model of mild, reproducible disc degeneration by an anulus needle puncture: correlation between the degree of disc injury and radiological and histological appearances of disc degeneration, Spine (Phila. Pa. 1976) 30 (2005) 5–14.

[27] D.M. Elliott, C.S. Yerramalli, J.C. Beckstein, J.I. Boxberger, W. Johannessen, E.J. Vresilovic, The effect of relative needle diameter in puncture and sham injection animal models of degeneration, Spine (Phila. Pa. 1976) 33 (2008) 588–596.

[28] M. Likhitpanichkul, M. Dreischarf, S. Illien-Junger, B. a. Walter, T. Nukaga, R.G. Long, D. Sakai, a. C. Hecht, J.C. Iatridis, Fibrin-genipin adhesive hydrogel for annulus fibrosus repair: performance evaluation with large animal organ culture, in situ biomechanics, and in vivo degradation tests, Eur. Cells Mater. 28 (2014) 25–38.

[29] R.G. Long, A. Bürki, P. Zysset, D. Eglin, D.W. Grijpma, S.B.G. Blanquer, A.C. Hecht, J.C. Iatridis, Mechanical restoration and failure analyses of a hydrogel and scaffold composite strategy for annulus fibrosus repair, Acta Biomater. 30 (2016) 116–125.

[30] D.A. Frauchiger, R.D. May, E. Bakirci, A. Tekari, S.C.W. Chan, M. Wöltje, L.M. Benneker, B. Gantenbein, Genipin-enhanced fibrin hydrogel and novel silk for intervertebral disc repair in a loaded bovine organ culture model, J. Funct. Biomater. 9 (2018).

[31] P. Grunert, B.H. Borde, S.B. Towne, Y. Moriguchi, K.D. Hudson, L.J. Bonassar, R. H??rtl, Riboflavin crosslinked high-density collagen gel for the repair of annular defects in intervertebral discs: an in vivo study, Acta Biomater. 26 (2015) 215–224.

[32] B. Pennicooke, I. Hussain, C. Berlin, S.R. Sloan, B. Borde, Y. Moriguchi, G. Lang, R. Navarro-Ramirez, J. Cheetham, L.J. Bonassar, R. Härtl, Annulus fibrosus repair using high-density collagen gel, Spine (Phila. Pa. 1976) 43 (2018) 208–215.

[33] P.-P. a Vergroesen, A.I. Bochyn Ska, K.S. Emanuel, S. Sharifi, I. Kingma, D.W. Grijpma, T.H. Smit, A biodegradable glue for annulus closure: evaluation of strength and endurance, Spine (Phila. Pa. 1976) 40 (2015) 622–628.

[34] F. Heuer, S. Ulrich, L. Claes, H.-J. Wilke, Biomechanical evaluation of conventional anulus fibrosus closure methods required for nucleus replacement, J. Neurosurg. Spine 9 (2008) 307–313.

[35] S.L. Parker, G. Grahovac, D. Vukas, M. Vilendecic, D. Ledic, M.J. McGirt, E.J. Carragee, Effect of an Annular closure device (Barricaid) on same-level recurrent disk herniation and disk height loss after primary lumbar discectomy: two-year results of a multicenter prospective cohort study, Clin. Spine Surg. 29 (2016) 454–460.

[36] W.J. Choy, K. Phan, A.D. Diwan, C.S. Ong, R.J. Mobbs, Annular closure device for disc herniation : meta-analysis of clinical outcome and complications, BMC Musculoskelet. Disord. 19 (2018) 1–9.

[37] M. Barth, C. Weiß, G.J. Bouma, R. Bostelmann, A. Kursumovic, J. Fandino, C. Thomé, Endplate changes after lumbar discectomy with and without implantation of an annular closure device, Acta Neurochir. 160 (2018) 855–862.

[38] E.H. Ledet, W. Jeshuran, J.C. Glennon, C. Shaffrey, P. De Deyne, C. Belden, B. Kallakury, A.L. Carl, Small intestinal submucosa for anular defect closure: long-term response in an in vivo sheep model, Spine (Phila. Pa. 1976) 34 (2009) 1457–1463.

[39] L. Xin, C. Zhang, F. Zhong, S. Fan, W. Wang, Z. Wang, Minimal invasive annulotomy for induction of disc degeneration and implantation of poly (lactic-co-glycolic acid) (PLGA) plugs for annular repair in a rabbit model, Eur. J. Med. Res. 21 (2016) 7.

[40] A.A. Hegewald, F. Medved, D. Feng, C. Tsagogiorgas, A. Beierfuß, G.A.K. Schindler, M. Trunk, C. Kaps, D.S. Mern, C. Thomé, Enhancing tissue repair in Annulus fibrosus defects of the intervertebral disc: analysis of a bio-integrative annulus implant in an in-vivo ovine model, J. Tissue Eng. Regenerat. Med. 9 (2015) 405–414.

[41] L. Koepsell, T. Remund, J. Bao, D. Neufeld, H. Fong, Y. Deng, Tissue engineering of Annulus fibrosus using electrospun fibrous scaffolds with aligned polycaprolactone fibers, J. Biomed. Mater. Res. Part A 99A (2011) 564–575.

[42] N. Wismer, S. Grad, G. Fortunato, S.J. Ferguson, M. Alini, D. Eglin, Biodegradable electrospun scaffolds for Annulus fibrosus tissue engineering: effect of scaffold structure and composition on Annulus fibrosus cells in vitro, Tissue Eng. Part A 20 (2014) 672–682.

[43] W. Johnson, A. Wootton, A. El Haj, Topographical guidance of intervertebral disc cell growth in vitro: towards the development of tissue repair strategies for the anulus fibrosus, Eur. Spine J. 15 (2006) S389–S396.

[44] E.F. Johnson, K. Chetty, I.M. Moore, a Stewart, W. Jones, The distribution and arrangement of elastic fibres in the intervertebral disc of the adult human, J. Anat. 135 (1982) 301–309.

[45] M.D. Humzah, R.W. Soames, Human intervertebral disc: structure and function, Structure 356 (1988) 337–356.

[46] S.B. Bruehlmann, J.B. Rattner, J.R. Matyas, N.A. Duncan, Regional variations in the cellular matrix of the Annulus fibrosus of the intervertebral disc, J. Anat. 201 (2002) 159–171.

[47] R.J. Errington, K. Puustjarvi, I.R. White, S. Roberts, J.P. Urban, Characterisation of cytoplasm-filled processes in cells of the intervertebral disc, J. Anat. 192 (1998) 369–378.

[48] L. Koepsell, L. Zhang, D. Neufeld, H. Fong, Y. Deng, Electrospun nanofibrous polycaprolactone scaffolds for tissue engineering of Annulus fibrosus, Macromol. Biosci. 11 (2011) 391–399.

[49] N.L. Nerurkar, D.M. Elliott, R.L. Mauck, Mechanical design criteria for intervertebral disc tissue engineering, J. Biomech. 43 (2010) 1017–1030.

[50] G. Chu, C. Shi, H. Wang, W. Zhang, H. Yang, B. Li, Strategies for Annulus fibrosus regeneration: from biological therapies to tissue engineering, Front. Bioeng. Biotechnol. 6 (2018) 1–13.

[51] M. Abedalwafa, F. Wang, L. Wang, C. Li, Biodegradable poly-epsilon-caprolactone (PCL) for tissue engineering applications: a review, Rev. Adv. Mater. Sci. 34 (2013) 123–140.

[52] M.A. Woodruff, D.W. Hutmacher, The return of a forgotten polymer - polycaprolactone in the 21st century, Prog. Polym. Sci. 35 (2010) 1217–1256.

[53] B. Dhandayuthapani, Y. Yoshida, T. Maekawa, D.S. Kumar, S. Sahoo, L.T. Ang, J.C. Goh, S.L. Toh, A. Cipitria, A. Skelton, T.R. Dargaville, P.D. Dalton, D.W. Hutmacher, Design, fabrication and characterization of PCL electrospun scaffolds—a review, J. Mater. Chem. 93 (2011) 1539–1550.

[54] N.L. Nerurkar, S. Sen, A.H. Huang, D.M. Elliott, R.L. Mauck, Engineered disc-like angle-ply structures for intervertebral disc replacement, Spine (Phila. Pa. 1976) 35 (2010) 867–873.

[55] N.L. Nerurkar, D.M. Elliott, R.L. Mauck, Mechanics of oriented electrospun nanofibrous scaffolds for Annulus fibrosus tissue engineering, Anticancer Res. 11 (2007) 1609–1612.

[56] N.L. Nerurkar, B.M. Baker, S. Sen, E.E. Wible, D.M. Elliott, R.L. Mauck, Nanofibrous biologic laminates replicate the form and function of the annulus fibrosus, Nat. Mater. 8 (2009) 986–992.

[57] J.T. Martin, A.H. Milby, J.A. Chiaro, D.H. Kim, N.M. Hebela, L.J. Smith, D.M. Elliott, R.L. Mauck, Translation of an engineered nanofibrous disc-like angle-ply structure for intervertebral disc replacement in a small animal model, Acta Biomater. 10 (2014) 2473–2481.

[58] A. Fotticchia, Y. Liu, E. Demirci, C. Lenardi, Electrospun polycaprolactone nanofibers support growth of human mesenchymal stem cells, 13th IEEE International Conference on Nanotechnology (IEEE-NANO 2013), 2013, pp. 158–161.

[59] T.P. Driscoll, R.H. Nakasone, S.E. Szczesny, D.M. Elliott, R.L. Mauck, Biaxial mechanics and inter-lamellar shearing of stem-cell seeded electrospun angle-ply laminates for annulus fibrosus tissue engineering, J. Orthop. Res. 31 (2013) 864–870.

[60] R. Kang, H. Li, Z. Xi, S. Ringgard, A. Baatrup, K. Rickers, M. Sun, D.Q.S. Le, M. Wang, L. Xie, Y. Xie, M. Chen, C. Bünger, Surgical repair of annulus defect with biomimetic multilamellar nano/microfibrous scaffold in a porcine model, J. Tissue Eng. Regenerat. Med. 12 (2018) 164–174.

[61] S.E. Gullbrand, B.G. Ashinsky, E.D. Bonnevie, D.H. Kim, J.B. Engiles, L.J. Smith, D.M. Elliott, T.P. Schaer, H.E. Smith, R.L. Mauck, Long-term mechanical function and integration of an implanted tissue-engineered intervertebral disc, Sci. Transl. Med. 10 (2018) 1–10.

[62] M. Fusellier, P. Colombier, J. Lesoeur, S. Youl, S. Madec, O. Gauthier, O. Hamel, J. Guicheux, J. Clouet, Longitudinal comparison of enzyme- and laser-treated intervertebral disc by MRI, X-ray, and histological analyses reveals discrepancies in the progression of disc degeneration: a rabbit study, BioMed Res. Int. 2016 (2016).

[63] L. Le Fournier, M. Fusellier, B. Halgand, J. Lesoeur, O. Gauthier, P. Menei, C. Montero-Menei, J. Guicheux, J. Clouet, The transpedicular surgical approach for the development of intervertebral disc targeting regenerative strategies in an ovine model, Eur. Spine J. 26 (2017) 2072–2083.

[64] M. Fusellier, J. Clouet, O. Gauthier, C. Le Visage, J. Guicheux, Animal models and imaging of intervertebral disc degeneration, Book Gene and Cell Delivery for Intervertebral Disc Degeneration, CRC Press, 2017.

[65] J.T. Martin, D.J. Gorth, E.E. Beattie, B.D. Harfe, L.J. Smith, D.M. Elliott, Needle puncture injury causes acute and long-term mechanical deficiency in a mouse model of intervertebral disc degeneration, J. Orthop. Res. 31 (2013) 1276–1282.

[66] H. Liang, S.Y. Ma, G. Feng, F.H. Shen, X. Joshua Li, Therapeutic effects of adenovirus-mediated growth and differentiation factor-5 in a mice disc degeneration model induced by annulus needle puncture, Spine J. 10 (2010) 32–41.

[67] G. Keorochana, J.S. Johnson, C.E. Taghavi, J.C. Liao, K.B. Lee, J.H. Yoo, S.S. Ngo, J.C. Wang, The effect of needle size inducing degeneration in the rat caudal disc: evaluation using radiograph, magnetic resonance imaging, histology, and immunohistochemistry, Spine J. 10 (2010) 1014–1023.

[68] K.D. Hudson, M. Alimi, P. Grunert, R. Härtl, L.J. Bonassar, Recent advances in biological therapies for disc degeneration: tissue engineering of the annulus fibrosus, nucleus pulposus and whole intervertebral discs, Curr. Opin. Biotechnol. 24 (2013) 872–879.

[69] R. Long, O. Torre, W. Hom, D. Assael, J. Iatridis, Design requirements for annulus fibrosus repair: review of forces, displacements and material properties of the intervertebral disc and a summary of candidate hydrogels for repair, J. Biomech. Eng. 138 (2016) 1–14.

[70] M. Yeganegi, R. a. Kandel, J.P. Santerre, Characterization of a biodegradable electrospun polyurethane nanofiber scaffold: mechanical properties and cytotoxicity, Acta Biomater. 6 (2010) 3847–3855.

[71] R. Kang, D.Q. Svend Le, H. Li, H. Lysdahl, M. Chen, F. Besenbacher, C. Bünger, Engineered three-dimensional nanofibrous multi-lamellar structure for annulus fibrosus repair, J. Mater. Chem. B 1 (2013) 5462–5468.

[72] M. Bhattacharjee, S. Miot, A. Gorecka, K. Singha, M. Loparic, S. Dickinson, A. Das, N.S. Bhavesh, A.R. Ray, I. Martin, S. Ghosh, Oriented lamellar silk fibrous scaffolds to drive cartilage matrix orientation: towards Annulus fibrosus tissue engineering, Acta Biomater. 8 (2012) 3313–3325.

[73] C.P. Barnes, S. a. Sell, E.D. Boland, D.G. Simpson, G.L. Bowlin, Nanofiber technology: designing the next generation of tissue engineering scaffolds, Adv. Drug Deliv. Rev. 59 (2007) 1413–1433.

[74] Y. Liu, Y. Ji, K. Ghosh, R.A.F. Clark, L. Huang, M.H. Rafailovich, Effects of fiber orientation and diameter on the behavior of human dermal fibroblasts on electrospun PMMA scaffolds, J. Biomed. Mater. Res. - Part A 90 (2009) 1092–1106.

[75] B.M. Baker, R.L. Mauck, The effect of nanofiber alignment on the maturation of engineered meniscus constructs, Biomaterials 28 (2007) 1967–1977.

[76] C. Liu, C. Zhu, J. Li, P. Zhou, M. Chen, H. Yang, B. Li, The effect of the fibre orientation of electrospun scaffolds on the matrix production of rabbit annulus fibrosus-derived stem cells, Bone Res 3 (2015) 15012.

[77] C. Zhu, J. Li, C. Liu, P. Zhou, H. Yang, B. Li, Modulation of the gene expression of annulus fibrosus-derived stem cells using poly (ether carbonate urethane) urea scaffolds of tunable elasticity, Acta Biomater. 29 (2016) 228–238.

[78] J.-F. Nisolle, B. Bihin, N. Kirschvink, F. Neveu, P. Clegg, A. Dugdale, X. Wang, J.-M. Vandeweerd, Prevalence of age-related changes in ovine lumbar intervertebral discs during computed tomography and magnetic resonance imaging, Comp. Med. 66 (2016) 300–307.

[79] H.-J. Wilke, A.A. Kettler, L.E. Claes, Are sheep spines a valid biomechanical model for Human spines, Spine (Phila. Pa. 1976) 22 (1997) 2365–2374.

[80] J.L. Bron, A.J. Van Der Veen, M.N. Helder, B.J. Van Royen, T.H. Smit, Biomechanical and in vivo evaluation of experimental closure devices of the Annulus fibrosus designed for a goat nucleus replacement model, Eur. Spine J. 19 (2010) 1347–1355.

[81] Y. Moriguchi, R. Navarro, P. Grunert, J. Mojica, K. Hudson, T. Khair, M. Alimi, L. Bonassar, R. Hartl, Total disc replacement using tissue- engineered intervertebral discs in the canine cervical, Spine 1 (2016) 1–18.

[82] D. Hampton, G. Laros, R. McCarron, D. Franks, Healing potential of the annulus fibrosus, Spine (Phila. Pa. 1976) 14 (1989) 398–401.

[83] O.L. Osti, B. Vernon-Roberts, R.D. Fraser, Volvo award in experimental studies. Annulus tears and intervertebral disc degeneration. An experimental study using an animal model, Spine (Phila. Pa. 1976) 15 (1990) 762–767 (1990).

[84] N.L. Fazzalari, J.J. Costi, T.C. Hearn, R.D. Fraser, B. Vernon-Roberts, J. Hutchinson, B. a Manthey, I.H. Parkinson, C. Sinclair, Mechanical and pathologic consequences of induced concentric anular tears in an ovine model, Spine (Phila. Pa. 1976) 26 (2001) 2575–2581.